

Ultrahigh energy storage density in epitaxial AlN/ScN superlattices

Zhijun Jiang,^{1,2,3} Bin Xu,^{4,*} Hongjun Xiang,^{2,5,6,†} and L. Bellaiche³

¹MOE Key Laboratory for Nonequilibrium Synthesis and Modulation of Condensed Matter,
School of Physics, Xi'an Jiaotong University, Xi'an 710049, China

²Key Laboratory of Computational Physical Sciences (Ministry of Education),
State Key Laboratory of Surface Physics, and Department of Physics, Fudan University, Shanghai 200433, China

³Physics Department and Institute for Nanoscience and Engineering,
University of Arkansas, Fayetteville, Arkansas 72701, USA

⁴Jiangsu Key Laboratory of Thin Films, School of Physical Science and Technology, Soochow University, Suzhou 215006, China

⁵Collaborative Innovation Center of Advanced Microstructures, Nanjing 210093, China

⁶Shanghai Qi Zhi Institute, Shanghai 200232, China

Dielectric and antiferroelectric materials are particularly promising for high-power energy-storage applications. However, relatively low energy density greatly hinders their usage in storage technologies. Here, we report first-principles-based calculations predicting that epitaxial and initially non-polar AlN/ScN superlattices can achieve an ultrahigh energy density of up to 200 J/cm³, accompanied by an ideal efficiency of 100%. We also show that high energy density requires the system being neither too close nor too far from a ferroelectric phase transition under zero electric field. A phenomenological model is further proposed to rationalize such striking features.

Electrostatic capacitors that are based on dielectric or antiferroelectric materials are promising energy storage components in various electronic applications because of their higher power density, faster charging/discharging rates, and better stability when compared with supercapacitors and batteries [1–16]. However, their relatively low energy density is the main bottleneck towards energy-storage applications, while intensive efforts have been devoted to find novel compounds with improved storage properties. In general, the recoverable energy density (U_{rec}) is determined by the work done by the electric field during discharging, $U_{\text{rec}} = \int_{P_r}^{P_{\text{max}}} E dP$, where P_{max} and P_r are the maximum and remnant polarization, respectively. To achieve high energy density, it is usually required to have high P_{max} , low P_r , and high breakdown strength [5–10]. The efficiency is defined as $\eta = [U_{\text{rec}}/(U_{\text{rec}} + U_{\text{loss}})] \times 100\%$, where U_{loss} is the energy loss density. Therefore, a linear dielectric material has an energy density (U) of $U = \frac{1}{2}\epsilon_0\epsilon_r E^2$, where ϵ_0 is the vacuum permittivity, ϵ_r is the relative permittivity, and E is the electric field. Obviously, high values of permittivity ϵ_r and breakdown strength E_{break} lead to large energy density [17–19]. On the other hand, nonlinear dielectrics – usually including ferroelectrics, antiferroelectric, and relaxors – have either low energy density (in ferroelectrics) or dissipative energy losses that can reduce efficiency (in antiferroelectrics and relaxors). For instance, the energy density is low for a ferroelectric material, due to large remnant polarization [19].

To maximize both energy density and efficiency, one can in fact imagine a nonlinear type dielectric material that can combine the advantages of a ferroelectric and a linear dielectric, i.e., possessing large polarization under high field, and being nonpolar under zero field as well as reversible. This would require the nonlinear dielectrics to have large ϵ_r and high E_{break} [11–16]. A promising candidate is the III-V semiconductor-based systems made by mixing AlN and ScN to form $\text{Al}_{1-x}\text{Sc}_x\text{N}$ solid solutions or AlN/ScN superlattices,

that have been attracting much attention due to their potential for high piezoelectric and electro-optic responses [20–29]. Note that a recent experiment observed a ferroelectric switching in $\text{Al}_{1-x}\text{Sc}_x\text{N}$ films, with a remnant polarization reaching a very large value – in excess of 1.0 C/m² [25] – which contrasts with the case of pure AlN that is of wurtzite-type structure [30, 31] and is polar but not ferroelectric. Note that for larger Sc compositions (above 43%), $\text{Al}_{1-x}\text{Sc}_x\text{N}$ can be non-polar [20, 21, 25].

The aim of this Letter is to demonstrate and explain why very promising energy-storage can be achieved in (Al,Sc)N systems being initially in a non-polar phase but at close proximity with a ferroelectric state that is easy to reach under electric fields.

Here, first-principles calculations are performed on (001) epitaxial 1×1 AlN/ScN superlattices within the local density approximation (LDA) to the density functional theory (DFT), as implemented in the ABINIT package [32]. The epitaxial strain is defined as $\eta_{\text{in}} = (a - a_{\text{eq}})/a_{\text{eq}}$, where a_{eq} is the in-plane lattice constant corresponding to the equilibrium $P\bar{6}m2$ phase of bulk 1×1 AlN/ScN superlattices [27]. A $6 \times 6 \times 4$ k -point mesh and a plane-wave kinetic energy cutoff of 50 Hartree and of 60 Hartree are employed for structural relaxation. The higher value of 60 Hartree is used to minimize the Pulay error in the stress. A dc electric field, E , is applied along the [001] direction (c -axis) by adopting the method developed in Refs. [33–36]. For each field-induced structure, the electrical polarization, P , along the c -axis is computed from the Berry phase method [37, 38] and P - E curves are then obtained. Note that, for each chosen strain and applied dc electric field, the in-plane lattice vectors are kept fixed during the simulations while the out-of-plane lattice vector and atomic positions are fully relaxed, until the force on each atom is smaller than 10^{-6} Hartree/Bohr – in order to simulate *epitaxial* films under electric field.

Due to Landauer's paradox, the theoretical electric field is

typically larger compared with measurement [9, 39–42], and the electric fields considered in this Letter have been rescaled by a factor of 1/3, in order that the P - E loop of the 1×1 AlN/ScN system under a -3% strain matches the experimental one corresponding to a $\text{Al}_{0.57}\text{Sc}_{0.43}\text{N}$ film [25] – as demonstrated in Fig. S1 of the Supplemental Material (SM) [43]. Note that such rescaling of computational electric fields is material-dependent but not phase-dependent for a given material [39]. For instance, Ref. [39] demonstrated that a rescaling of the electric field is able to reproduce very well the electric field-*versus*-temperature phase diagram of the complex $\text{Pb}(\text{Mg},\text{Nb})\text{O}_3$ system, with this phase diagram involving different phases (e.g., relaxor paraelectric *versus* ferroelectric) and even different orders (first *versus* second) of the phase transitions. Regarding the magnitude of the (renormalized) fields to be considered here, it is first worthwhile to indicate that a recent experiment reported a feasible electric field as high as $\simeq 5$ MV/cm in $\text{Al}_{1-x}\text{Sc}_x\text{N}$ films [25]. Moreover, one can also estimate the intrinsic breakdown field of such systems empirically, which depends on the band gap [50]. Our predicted gap of 3.1 eV after correction (to account for the typical underestimation of LDA) of the 1×1 AlN/ScN superlattice ground state [27] yields an intrinsic breakdown field, E_{break} , of 6.3 MV/cm, which will be the maximum fields considered here. Note that the estimated breakdown field is reasonable since (1) Yazawa *et al.* reported the highest applied electric field (~ 6 MV/cm) in epitaxial $\text{Al}_{0.7}\text{Sc}_{0.3}\text{N}$ film [28]; and (2) Yasuoka *et al.* also reported very large coercive fields of the order of 4–7 MV/cm and maximum applicable electric fields of the order 5–10 MV/cm in $\text{Al}_{1-x}\text{Sc}_x\text{N}$ films [29]. We also used another method [47, 48] to estimate the intrinsic breakdown field, which provides a value of ~ 6.59 MV/cm, that is rather close to the 6.3 MV/cm field used in our manuscript (see the SM [43]).

For the 1×1 AlN/ScN superlattices under different epitaxial strains, previous studies have predicted the existence of different phases [26, 27], including a wurtzite-derived structure (polar $P3m1$ space group with a polarization along the c -axis) and a hexagonal-derived structure (non-polar $P\bar{6}m2$ space group). They are related to each other by a continuous change in the internal parameter (u) and the axial ratio (c/a) [27]. Figure 1(a) shows the P - E curves for strain values larger than -0.5% (from compressive to tensile), with the hexagonal-derived structure as ground state [see Fig. 1(b) for such structure at 1% strain under zero field]. The structure associated with the electric field of 5 MV/cm is polar and close to the wurtzite-derived structure [see Fig. 1(c)].

When the strain is between -5% and -1% (as shown in Fig. S1(b) of the SM [43]), the P - E loops show typical single hysteresis of ferroelectrics with switching of polarization between the two degenerate wurtzite-derived structures, and the magnitudes of the critical fields depend very strongly on strain. Similar strong dependency was also observed in $\text{Al}_{1-x}\text{Sc}_x\text{N}$ solid solutions with respect to the Sc composition [25]; therefore, it suggests that varying composition in the solid solution or changing the strain for a fixed alloy or

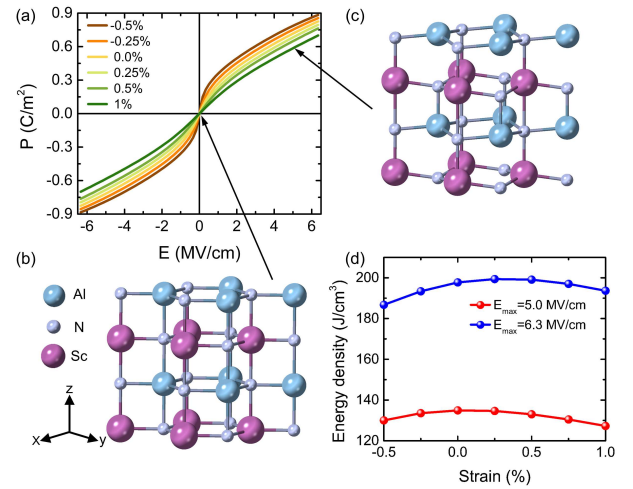


FIG. 1. (a) P - E hysteresis curves with different epitaxial strains with the ground state being a hexagonal-derived structure in 1×1 AlN/ScN superlattices. Crystal structures of 1% tensile strain under electric fields of (b) 0 MV/cm and (c) 5 MV/cm, respectively, in 1×1 AlN/ScN superlattices. (d) Energy density versus misfit strain for two different ending electric fields of 5.0 MV/cm and 6.3 MV/cm.

superlattice may involve similar physics. Due to the strong strain dependency, the hysteresis rapidly shrinks with reduced compressive strain, and completely vanishes beyond -0.5% strain, as depicted in Fig. 1(a). In this range of strains, the ground state becomes the non-polar $P\bar{6}m2$ hexagonal-derived phase. More interestingly, the P - E curve is very nonlinear at small compressive strain (e.g., -0.5%) – starting with large dielectric susceptibility at small field and saturating at elevated field – while it becomes more linear as the strain increases (e.g., 1%). And the transition to the polar wurtzite-type phase is predicted to be continuous and fully reversible upon increasing and decreasing electric fields.

Let us now check the energy storage properties for the 1×1 AlN/ScN superlattices for misfit strains varying between -0.5% to $+1\%$. The first feature to realize is that the energy efficiency is automatically 100% because the charging and discharging processes are completely reversible, as revealed by the continuous P - E curves of Fig. 1(a). The energy density is depicted in Fig. 1(d) for epitaxial strain ranging between -0.5% and $+1\%$, with the maximal applied electric field being 5 MV/cm that has been realized experimentally [25] in this type of nitride semiconductors, and 6.3 MV/cm estimated as the intrinsic breakdown field. It is striking that the energy density reaches (slightly strain-dependent) values varying between 127 and 135 J/cm³ and between 187 and 200 J/cm³ when using 5 MV/cm and 6.3 MV/cm for the largest applied field, respectively. All these energy densities and efficiencies are thus predicted to be giant, since they are much larger than those measured in lead-based and lead-free dielectric thin films [6, 12, 14, 15, 51–54], such as $(\text{Bi}_{0.5}\text{Na}_{0.5})_{0.9118}\text{La}_{0.02}\text{Ba}_{0.0582}(\text{Ti}_{0.97}\text{Zr}_{0.03})\text{O}_3$ (BNLBTZ) epitaxial relaxor (154 J/cm³ and 97% for a maximum ap-

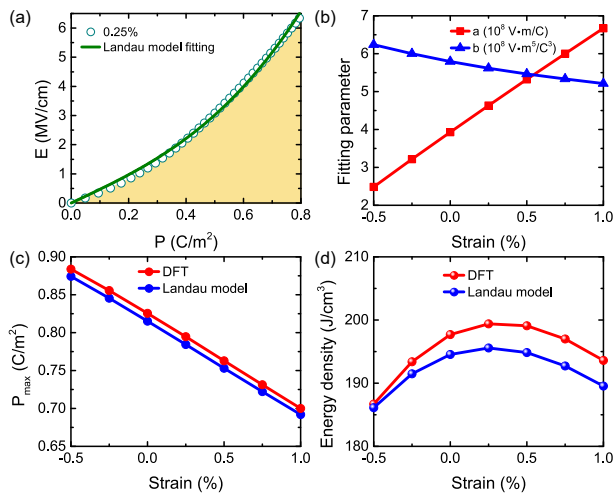


FIG. 2. (a) Electric field versus polarization for strains at 0.25% (the solid green line represents the fit of the DFT results by the Landau model), with the yellow area showing the energy density. (b) Evolution with strain of fitting parameters a and b (see text). Strain-dependence of (c) P_{\max} and (d) energy density results obtained from DFT and Landau model. These data correspond to a maximal applied electric field of $E_{\text{break}} = 6.3$ MV/cm.

plied field, $E_{\max} = 3.5$ MV/cm [6], BiFeO₃-BaTiO₃-SrTiO₃ solid solutions (112 J/cm³ and 80% for $E_{\max} = 4.9$ MV/cm) [12], Pb_{0.88}Ca_{0.12}ZrO₃ (91.3 J/cm³ and 85.3% for $E_{\max} = 5$ MV/cm) [14], and ion-bombarded relaxor ferroelectric 0.68Pb(Mg_{1/3}Nb_{2/3})O₃-0.32PbTiO₃ (PMN-PT) films (133 J/cm³ and 75% for $E_{\max} = 5.9$ MV/cm) [15]. The 100% efficiency and the giant energy densities suggest that the 1×1 AlN/ScN superlattices are highly promising for energy-storage applications.

To understand these results, let us recall that, a nonlinear dielectric with no energy dissipation has an energy density U has the following form:

$$U = \int_0^{P_{\max}} E dP, \quad (1)$$

where P_{\max} is the maximum polarization, exhibited at the highest applied field, E_{\max} . Figure 2(a) displays the (positive) electric field applied along the [001] pseudo-cubic direction as a function of polarization for one particular misfit strain at 0.25%. The area shown in yellow of Fig. 2(a) is the energy density.

The energy density in Fig. 1(d) can be understood based on a simple Landau-type free energy that describes the behavior of a nonlinear dielectric:

$$F = \frac{1}{2}aP^2 + \frac{1}{4}bP^4 - EP, \quad (2)$$

where a and b are coefficients of the quadratic and quartic terms, respectively, and they are positively defined for a paraelectric or non-polar phase.

Noting that at equilibrium condition, we have $\frac{\partial F}{\partial P} = 0$, which leads to

$$E = aP + bP^3. \quad (3)$$

Thus, the polarization is zero without the application of an electric field. Consequently, the energy density can be written in the simple following form:

$$U = \int_0^{P_{\max}} (aP + bP^3) dP = \frac{1}{2}aP_{\max}^2 + \frac{1}{4}bP_{\max}^4. \quad (4)$$

As shown in Fig. 2(a), the electric field versus polarization (E - P) data for strains at 0.25% can be very well fitted by Eq. (3). In fact, Eq. (3) fits remarkably well the DFT E - P data for all the considered strain ranging between -0.5% and $+1\%$ (see Fig. S3 of the SM [43]). Figure 2(b) shows the fitting parameters a and b as a function of epitaxial strain ranging between -0.5% and $+1\%$, for electric fields up to the intrinsic breakdown field $E_{\max} = E_{\text{break}} = 6.3$ MV/cm. Interestingly, Fig. 2(b) reveals that the fitting parameter a linearly increases when the strain increases from -0.5% to $+1\%$ (a varies from 2.5×10^8 V·m/C to 6.7×10^8 V·m/C). In contrast, the b parameter linearly decreases with strain, with the change of b being much smaller in percentage than a and taking values ranging between 6.2×10^8 V·m⁵/C³ and 5.2×10^8 V·m⁵/C³. Note that the a parameter of the Landau expansion is negative in our phenomenology model when the ground state of the superlattice is ferroelectric (see Fig. S4 of the SM [43]).

Figure 2(c) displays the value of the polarization, P_{\max} , for $E_{\max} = 6.3$ MV/cm, as a function of strain both from DFT calculations and the Landau model using the DFT-fitted a and b in Eq. (3). One can first clearly see that, for any of these strains, the DFT and Landau model provide nearly identical results. According to Fig. 2(c), P_{\max} is larger than 0.7 C/m² for any considered strain ranging between -0.5% and $+1\%$, which reflects that the structure at such high field is wurtzite-like. Note that, for $E_{\max} = E_{\text{break}}$, P_{\max} linearly decreases with strain from 0.88 to 0.70 C/m², which can be simply understood by the fact that increasing strains towards and within the tensile regime is known to reduce the out-of-plane polarization in ferroelectric systems [26, 55, 56].

To understand the results in Fig. 1(d), we use Eq. (4) to obtain the energy density for different strains at $E_{\max} = 6.3$ MV/cm. Figure 2(d) shows that the Landau model agrees rather well with the DFT-obtained energy density, with an excellent agreement at small strain and a slightly increasing discrepancy at larger strains (less than 2% at 1.0% strain), implying the validity of the Landau model. Equation (4) tells us that the energy density is the sum of two terms – that are $\frac{1}{2}aP_{\max}^2$ and $\frac{1}{4}bP_{\max}^4$. The first contribution depends on the product of the a parameter and P_{\max}^2 , and is numerically found to increase when the strain is enhanced between -0.5% and $+1\%$ (see Fig. S5 of the SM [43]). The second contribution is the product between the b parameter and P_{\max}^4 , and decreases

with strain since b slightly decreases when changing the strain from -0.5% to $+1\%$ while P_{\max} is reduced with strain, as a consequence of the aforementioned coupling between out-of-plane polarization and in-plane strains [see Figs. 2(b) and 2(c)]. Practically, the contribution of $\frac{1}{2}aP_{\max}^2$ (respectively, of $\frac{1}{4}bP_{\max}^4$) to the total energy density is 51% (respectively, 49%), 73% (respectively, 27%), and 84% (respectively, 16%) for strains at -0.5% , 0.25% , and 1% , respectively. Note also that the strain dependency of $\frac{1}{2}aP_{\max}^2$ and $\frac{1}{4}bP_{\max}^4$, along with the dependency of P_{\max} on E_{\max} [see Fig. 1(a)], leads to a maximum value of the total energy density U occurring at a specific strain for a given E_{\max} , while different E_{\max} can further quantitatively modulate the performance. For instance, such maximum occurs at 0% and 0.25% misfit strain when the largest applied field is 5 MV/cm and 6.3 MV/cm , respectively [see Fig. 1(d)].

As evidenced above, we numerically found that the energy density at its maximum value, for our selected E_{\max} of 6.3 MV/cm , mostly (i.e., at 73%) depends on the a parameter and P_{\max} via $\frac{1}{2}aP_{\max}^2$. Let us thus fix b as a constant and vary the a parameter for the case of $E_{\max} = 6.3 \text{ MV/cm}$, and compute the resulting P_{\max} and energy density using Eqs. (3) and (4). The results are shown in Fig. S6 of the SM [43], which reveal that the energy density varies non-monotonically with the a parameter at a selected strain of 0.25% , presenting a maximum, $U_{\max, b\text{-fixed}}$, for an intermediate a value. Note that small a gives smaller density than $U_{\max, b\text{-fixed}}$ because $\frac{1}{2}aP_{\max}^2$ is reduced via the a parameter; while larger a also provides an energy density being smaller than $U_{\max, b\text{-fixed}}$ because now P_{\max} is weakened in $\frac{1}{2}aP_{\max}^2$. These facts automatically imply that there is a trade-off to have large energy density: the system should not be too close (i.e., should not have a very small a) but also not be too far (i.e., should not possess a too large a) from a ferroelectric phase transition.

In summary, we have performed first-principles calculations to investigate the energy-storage properties and out-of-plane strains in epitaxial $1 \times 1 \text{ AlN/ScN}$ superlattices. We find that these systems exhibit very high energy-densities up to 200 J/cm^3 and an ideal 100% efficiency. Interestingly, we also found that such systems can simultaneously exhibit ultrahigh strain levels of about 10%, as detailed in the SM [43]. Note that InN can be used as a substrate to get 0.3% of strain [27] to achieve the predicted performance, which is promising for energy storage in our proposed system. Such unusual and promising features originate from high values of the electric field that can be applied in these systems, and in particular from a nonlinear electric-field-induced strong polarizability of the non-polar hexagonal-like polymorph. A simple Landau model is developed to analyze and understand these results, which also suggests that (Al,Sc)N disordered solid solutions should also possess these “wunderbar” properties for compositions lying in the non-polar regime near but not too close to the border with the wurtzite-like structure. The proposed new concept of using nonlinear and non-polar systems close to a ferroelectric state as an energy storage material is general and we expect that other materials with similar characteristics are

also good candidates for energy storage.

This work is supported by the National Natural Science Foundation of China (Grants No. 11804138, No. 11825403, and No. 11991061), Shandong Provincial Natural Science Foundation (Grant No. ZR2019QA008), China Postdoctoral Science Foundation (Grants No. 2020T130120 and No. 2018M641905), and “Young Talent Support Plan” of Xi’an Jiaotong University (Grant No. WL6J004). B.X. acknowledges financial support from National Natural Science Foundation of China under Grant No. 12074277 and Natural Science Foundation of Jiangsu Province (BK20201404), the startup fund from Soochow University, and the support from Priority Academic Program Development (PAPD) of Jiangsu Higher Education Institutions. L.B. acknowledges the DARPA grant HR0011-15-2-0038 (MATRIX program). The Arkansas High Performance Computing Center (AHPCC) of University of Arkansas and HPC Platform of Xi’an Jiaotong University are also acknowledged.

* binxu19@suda.edu.cn

† hxiang@fudan.edu.cn

- [1] B. Chu, X. Zhou, K. Ren, B. Neese, M. Lin, Q. Wang, F. Bauer, and Q. M. Zhang, A Dielectric Polymer with High Electric Energy Density and Fast Discharge Speed, *Science* **313**, 334 (2006).
- [2] X. Hao, A review on the dielectric materials for high energy-storage application, *J. Adv. Dielectr.* **3**, 1330001 (2013).
- [3] S. Patel, A. Chauhan, and R. Vaish, Enhancing electrical energy storage density in anti-ferroelectric ceramics using ferroelastic domain switching, *Mater. Res. Express* **1**, 045502 (2014).
- [4] Q. Li, L. Chen, M. R. Gadinski, S. Zhang, G. Zhang, H. U. Li, E. Iagodkine, A. Haque, L.-Q. Chen, T. N. Jackson, and Q. Wang, Flexible high-temperature dielectric materials from polymer nanocomposites, *Nature (London)* **523**, 576 (2015).
- [5] A. Chauhan, S. Patel, R. Vaish, and C. R. Bowen, Anti-Ferroelectric Ceramics for High Energy Density Capacitors, *Materials* **8**, 8009 (2015).
- [6] B. Peng, Q. Zhang, X. Li, T. Sun, H. Fan, S. Ke, M. Ye, Y. Wang, W. Lu, H. Niu, J. F. Scott, X. Zeng, and H. Huang, Giant Electric Energy Density in Epitaxial Lead-Free Thin Films with Coexistence of Ferroelectrics and Antiferroelectrics, *Adv. Electron. Mater.* **1**, 1500052 (2015).
- [7] Prateek, V. K. Thakur, and R. K. Gupta, Recent Progress on Ferroelectric Polymer-Based Nanocomposites for High Energy Density Capacitors: Synthesis, Dielectric Properties, and Future Aspects, *Chem. Rev.* **116**, 4260 (2016).
- [8] Z. Yao, Z. Song, H. Hao, Z. Yu, M. Cao, S. Zhang, M. T. Lagan, and H. Liu, Homogeneous/Inhomogeneous-Structured Dielectrics and their Energy-Storage Performances, *Adv. Mater.* **29**, 1601727 (2017).
- [9] B. Xu, J. Íñiguez, and L. Bellaiche, Designing lead-free antiferroelectrics for energy storage, *Nat. Commun.* **8**, 15682 (2017).
- [10] H. Huang and J. F. Scott, *Ferroelectric Materials for Energy Applications* (Wiley, Weinheim, 2018).
- [11] L. Yang, X. Kong, F. Li, H. Hao, Z. Cheng, H. Liu, J.-F. Li, and S. Zhang, Perovskite lead-free dielectrics for energy storage applications, *Prog. Mater. Sci.* **102**, 72 (2019).
- [12] H. Pan, F. Li, Y. Liu, Q. Zhang, M. Wang, S. Lan, Y. Zheng, J.

- Ma, L. Gu, Y. Shen, P. Yu, S. Zhang, L.-Q. Chen, Y.-H. Lin, and C.-W. Nan, Ultrahigh-energy density lead-free dielectric films via polymorphic nanodomain design, *Science* **365**, 578 (2019).
- [13] K. Zou, Y. Dan, H. Xu, Q. Zhang, Y. Lu, H. Huang, and Y. He, Recent advances in lead-free dielectric materials for energy storage, *Mater. Res. Bull.* **113**, 190 (2019).
- [14] Y. Z. Li, J. L. Lin, Y. Bai, Y. X. Li, Z. D. Zhang, and Z. J. Wang, Ultrahigh-Energy Storage Properties of (PbCa)ZrO₃ Antiferroelectric Thin Films via Constructing a Pyrochlore Nanocrystalline Structure, *ACS Nano* **14**, 6857 (2020).
- [15] J. Kim, S. Saremi, M. Acharya, G. Velarde, E. Parsonnet, P. Donahue, A. Qualls, D. Garcia, and L. W. Martin, Ultrahigh capacitive energy density in ion-bombarded relaxor ferroelectric films, *Science* **369**, 81(2020).
- [16] M. Peddigari, H. Palneedi, G.-T. Hwang, and J. Ryu, Linear and Nonlinear Dielectric Ceramics for High-Power Energy Storage Capacitor Applications, *J. Korean Ceram. Soc.* **56**, 1 (2019).
- [17] H. Y. Zhou, X. N. Zhu, G. R. Ren, and X. M. Chen, Enhanced energy storage density and its variation tendency in CaZr_xTi_{1-x}O₃ ceramics, *J. Alloys Compd.* **688**, 687 (2016).
- [18] H. Y. Zhou, X. Q. Liu, X. L. Zhu, and X. M. Chen, CaTiO₃ linear dielectric ceramics with greatly enhanced dielectric strength and energy storage density, *J. Am. Ceram. Soc.* **101**, 1999 (2018).
- [19] Q. Li, F.-Z. Yao, Y. Liu, G. Zhang, H. Wang, and Q. Wang, High-Temperature Dielectric Materials for Electrical Energy Storage, *Annu. Rev. Mater. Res.* **48**, 219 (2018).
- [20] M. Akiyama, T. Kamohara, K. Kano, A. Teshigahara, Y. Takeuchi, and N. Kawahara, Enhancement of Piezoelectric Response in Scandium Aluminum Nitride Alloy Thin Films Prepared by Dual Reactive Cosputtering, *Adv. Mater.* **21**, 593 (2009).
- [21] M. Akiyama, K. Kano, and A. Teshigahara, Influence of growth temperature and scandium concentration on piezoelectric response of scandium aluminum nitride alloy thin films, *Appl. Phys. Lett.* **95**, 162107 (2009).
- [22] F. Tasnádi, B. Alling, C. Höglund, G. Wingqvist, J. Birch, L. Hultman, and I. A. Abrikosov, Origin of the Anomalous Piezoelectric Response in Wurtzite Sc_xAl_{1-x}N Alloys, *Phys. Rev. Lett.* **104**, 137601 (2010).
- [23] S. Zhang, D. Holec, W. Y. Fu, C. J. Humphreys, and M. A. Moram, Tunable optoelectronic and ferroelectric properties in Sc-based III-nitrides, *J. Appl. Phys.* **114**, 133510 (2013).
- [24] P. Daoust, P. Desjardins, R. A. Masut, V. Gosselin, and M. Côté, Ab initio piezoelectric properties of Al_{0.5}Sc_{0.5}N: Impact of alloy configuration on the $d_{33,f}$ piezoelectric strain coefficient, *Phys. Rev. Mater.* **1**, 055402 (2017).
- [25] S. Fichtner, N. Wolff, F. Lofink, L. Kienle, and B. Wagner, AlScN: A III-V semiconductor based ferroelectric, *J. Appl. Phys.* **125**, 114103 (2019).
- [26] M. Noor-A-Alam, O. Z. Olszewski, and M. Nolan, Ferroelectricity and Large Piezoelectric Response of AlN/ScN Superlattice, *ACS Appl. Mater. Interfaces* **11**, 20482 (2019).
- [27] Z. Jiang, C. Paillard, D. Vanderbilt, H. Xiang, and L. Bellaiche, Designing Multifunctionality via Assembling Dissimilar Materials: Epitaxial AlN/ScN Superlattices, *Phys. Rev. Lett.* **123**, 096801 (2019).
- [28] K. Yazawa, D. Drury, A. Zakutayev, and G. L. Brenneka, Reduced coercive field in epitaxial thin film of ferroelectric wurtzite Al_{0.7}Sc_{0.3}N, *Appl. Phys. Lett.* **118**, 162903 (2021).
- [29] S. Yasuoka, T. Shimizu, A. Tateyama, M. Uehara, H. Yamada, M. Akiyama, Y. Hiranaga, Y. Cho, and H. Funakubo, Effects of deposition conditions on the ferroelectric properties of (Al_{1-x}Sc_x)N thin films, *J. Appl. Phys.* **128**, 114103 (2020).
- [30] A. F. Wright and J. S. Nelson, Consistent structural properties for AlN, GaN, and InN, *Phys. Rev. B* **51**, 7866 (1995).
- [31] C. Bungaro, K. Rapcewicz, and J. Bernholc, Ab initio phonon dispersions of wurtzite AlN, GaN, and InN, *Phys. Rev. B* **61**, 6720 (2000).
- [32] X. Gonze, J.-M. Beuken, R. Caracas, F. Detraux, M. Fuchs, G.-M. Rignanese, L. Sindic, M. Verstraete, G. Zerah, F. Jollet, M. Torrent, A. Roy, M. Mikami, Ph. Ghosez, J.-Y. Raty, and D. C. Allan, First-principles computation of material properties: the ABINIT software project, *Comput. Mater. Sci.* **25**, 478 (2002).
- [33] R. W. Nunes and D. Vanderbilt, Real-Space Approach to Calculation of Electric Polarization and Dielectric Constants, *Phys. Rev. Lett.* **73**, 712 (1994).
- [34] R. W. Nunes and X. Gonze, Berry-phase treatment of the homogeneous electric field perturbation in insulators, *Phys. Rev. B* **63**, 155107 (2001).
- [35] I. Souza, J. Íñiguez, and D. Vanderbilt, First-Principles Approach to Insulators in Finite Electric Fields, *Phys. Rev. Lett.* **89**, 117602 (2002).
- [36] J. W. Zwanziger, J. Galbraith, Y. Kipouros, M. Torrent, M. Giantomassi, X. Gonze, Finite homogeneous electric fields in the projector augmented wave formalism: Applications to linear and nonlinear response, *Comput. Mater. Sci.* **58**, 113 (2012).
- [37] R. D. King-Smith and D. Vanderbilt, Theory of polarization of crystalline solids, *Phys. Rev. B* **47**, 1651(R) (1993).
- [38] R. Resta, Macroscopic polarization in crystalline dielectrics: the geometric phase approach, *Rev. Mod. Phys.* **66**, 899 (1994).
- [39] Z. Jiang, Y. Nahas, S. Prokhorenko, S. Prosandeev, D. Wang, J. Íñiguez, and L. Bellaiche, Giant electrocaloric response in the prototypical Pb(Mg,Nb)O₃ relaxor ferroelectric from atomistic simulations, *Phys. Rev. B* **97**, 104110 (2018).
- [40] J. Lu, G. Chen, W. Luo, J. Íñiguez, L. Bellaiche, and H. Xiang, Ferroelectricity with Asymmetric Hysteresis in Metallic LiOsO₃ Ultrathin Films, *Phys. Rev. Lett.* **122**, 227601 (2019).
- [41] L. Chen, C. Xu, H. Tian, H. Xiang, J. Íñiguez, Y. Yang, and L. Bellaiche, Electric-Field Control of Magnetization, Jahn-Teller Distortion, and Orbital Ordering in Ferroelectric Ferromagnets, *Phys. Rev. Lett.* **122**, 247701 (2019).
- [42] Z. Jiang, C. Paillard, H. Xiang, and L. Bellaiche, Linear Versus Nonlinear Electro-Optic Effects in Materials, *Phys. Rev. Lett.* **125**, 017401 (2020).
- [43] See Supplemental Material at [URL will be inserted by publisher] for more details about (i) the renormalization factor of the theoretical electric fields; (ii) another method to estimate the intrinsic breakdown field; (iii) out-of-plane strain versus electric field; and (iv) using a simple Landau model to understand the energy storage results in 1×1 AlN/ScN superlattices.
- [44] S.-E. Park and T. R. Shrout, Ultrahigh strain and piezoelectric behavior in relaxor based ferroelectric single crystals, *J. Appl. Phys.* **82**, 1804 (1997).
- [45] B. Jaffe, W. R. Cook, and H. Jaffe, *Piezoelectric Ceramics* (Academic Press, London, 1971).
- [46] C. A. Randall, A. Kelnberger, G. Y. Yang, R. E. Eitel, and T. R. Shrout, High Strain Piezoelectric Multilayer Actuators—A Material Science and Engineering Challenge, *J. Electroceram.* **14**, 177 (2005).
- [47] C. Kim, G. Pilania, and R. Ramprasad, From Organized High-Throughput Data to Phenomenological Theory using Machine Learning: The Example of Dielectric Breakdown, *Chem. Mater.* **28**, 1304 (2016).
- [48] C. Kim, G. Pilania, and R. Ramprasad, Machine Learning Assisted Predictions of Intrinsic Dielectric Breakdown Strength of ABX₃ Perovskites, *J. Phys. Chem. C* **120**, 14575 (2016).
- [49] P. B. Perry and R. F. Rutz, The optical absorption edge of

- single-crystal AlN prepared by a close-spaced vapor process, *Appl. Phys. Lett.* **33**, 319 (1978).
- [50] L.-M. Wang, Relationship between Intrinsic Breakdown Field and Bandgap of Materials. *25th International Conference on Microelectronics* (Belgrade, 2006).
- [51] M. H. Park, H. J. Kim, Y. J. Kim, T. Moon, K. D. Kim, and C. S. Hwang, Thin $\text{Hf}_x\text{Zr}_{1-x}\text{O}_2$ Films: A New Lead-Free System for Electrostatic Supercapacitors with Large Energy Storage Density and Robust Thermal Stability, *Adv. Energy Mater.* **4**, 1400610 (2014).
- [52] B. Ma, Z. Hu, R. E. Koritala, T. H. Lee, S. E. Dorris, and U. Balachandran, PLZT film capacitors for power electronics and energy storage applications, *J. Mater. Sci. Mater. Electron.* **26**, 9279 (2015).
- [53] Z. Sun, C. Ma, M. Liu, J. Cui, L. Lu, J. Lu, X. Lou, L. Jin, H. Wang, and C.-L. Jia, Ultrahigh Energy Storage Performance of Lead-Free Oxide Multilayer Film Capacitors via Interface Engineering, *Adv. Mater.* **29**, 1604427 (2017).
- [54] H. Pan, J. Ma, J. Ma, Q. Zhang, X. Liu, B. Guan, L. Gu, X. Zhang, Y.-J. Zhang, L. Li, Y. Shen, Y.-H. Lin, and C.-W. Nan, Giant energy density and high efficiency achieved in bismuth ferrite-based film capacitors via domain engineering, *Nat. Commun.* **9**, 1813 (2018).
- [55] Y. Yang, W. Ren, M. Stengel, X. H. Yan, and L. Bellaiche, Revisiting Properties of Ferroelectric and Multiferroic Thin Films under Tensile Strain from First Principles, *Phys. Rev. Lett.* **109**, 057602 (2012).
- [56] L. Chen, Y. Yang, Z. Gui, D. Sando, M. Bibes, X. K. Meng, and L. Bellaiche, Large Elasto-Optic Effect in Epitaxial PbTiO_3 Films, *Phys. Rev. Lett.* **115**, 267602 (2015).